CHALLENGES OF PINPOINT LANDING FOR PLANETARY EXPLORATION : THE LION ABSOLUTE VISION-BASED NAVIGATION SYSTEM STEP-WISE VALIDATION APPROACH

Thomas Voirin[(1)], Jeff Delaune[(2)], G. Le Besnerais[(3)], J.L Farges[(4)]
Clément Bourdarias[(5)] and Hans Krueger[(6)]
[(1)] ESA, ESTEC Keplerlaan 1, 2200 AG Noordwijk (the Netherlands), Email:Thomas.voirin@esa.int
[(2)]ONERA, Systems Control and Flight Dynamics, 2 avenue Edouard Belin, 31000 Toulouse (France, Email:jeff.delaune@onera.fr
[(3)]ONERA, Modelling and Information Processing, Chemin de la Hunière, 91123 Palaiseau (France), Email:guy.le_besnerais@onera.fr
[(4)]ONERA, Systems Control and Flight Dynamics, 2 avenue Edouard Belin, 31000 Toulouse (France), Email:jean-loup.farges@onera.fr
[(5)]Astrium Space Transportation, 66 route de Verneuil, 78133 Les Mureaux (France), Email:clement.bourdarias@astrium.eads.net
[(6)] DLR Institute of Space Systems, GNC systems, Robert Hooke Strasse 7, 28359 Bremen (Germany), Email : hans.krueger@dlr.de

ABSTRACT

After ExoMars in 2016 and 2018, future ESA missions to Mars, the Moon, or asteroids will require *safe* and *pinpoint precision* landing capabilities, with for example a specified accuracy of typically 100 m at touchdown for a Moon landing. The *safe* landing requirement can be met thanks to state-of-the-art Terrain-Relative Navigation (TRN) sensors such as Wide-Field-of-View vision-based navigation cameras (VBNC), with appropriate hazard detection and avoidance algorithms. To reach the *pinpoint precision* requirement, on-board absolute navigation with respect to the landing site is mandatory, with a typical accuracy better than 100 m at touchdown for a Lunar mission, or below 10 km at entry interface for a Mars landing missions.

In this paper, we present the validation approach and experimental results of an Absolute Visual Navigation system (AVN) known as *Lion*. The *Lion* functional architecture will be first presented, as well as the implemented incremental validation and verification approach ; experimental set-up and end-to-end tests results will be summarized. Finally, way forward and lessons learned will be discussed.

1. CONTEXT

Various techniques are being currently explored by ESA and partners, based on visual recognition of known landmarks. Such options rely on the a priori identification of visual landmarks from previous orbital missions imagery (e.g. craters), co-registered with a high resolution Digital Elevation Map (DEM, also available from previous orbital missions) to generate a landmarks database, which will be used by the on-board vision-based navigation system as a surface map. So far, most of the developments have focused on the use of craters as visual landmarks, such as [2] ; however, craters may not be found on all planetary surfaces, and may limit the use of such algorithms to areas where at least 3 to 4 sharp craters are in visibility ; for the Moon, this limits its altitude of use to several km.

Other techniques have been investigated, based on the use of typical image processing features such as Harris corners with dedicated descriptors. LandStel [3] for instance has investigated the use of geometrical descriptors (an approach similar to the Star Tracker acquisition algorithms) for matching purpose, showing promising results ; however, the technique was assuming all features were lying on a flat planar surface to re-project the features scale globally on the image, hence discarding its use as-is over terrains with significant topography variations, such as a significant portion of the Moon at low altitude), or with spherical appearance (such as for orbit and planetary approach.

The Lion activity, which is co-funded by ESA, ASTRIUM and ONERA, proposes an alternative approach which is generic enough to be applicable to potentially all future planetary landing missions, provided accurate imagery and DEM of these planetary surfaces have been gathered by previous orbital missions (which is already the case for the Moon and for Mars). *Lion* relies on the use of generic visual

landmarks (Harris-Laplace points), and is able to cope with any 3D topography. Scale invariance is efficiently employed through the scale of each landmark as an additional matching parameter. *Lion* includes the design and prototyping of the precision landing navigation system, primarily developed for a Lunar precision landing scenario, and its incremental validation through simulation (virtual images), hardware-in-the-loop testing on a Moon-analogue planetary mock-up (known as VisiLab and built and hosted at ESA ESTEC), and then test flight onto ONERA's RESSAC UAV.

This step-wise process implemented in this activity has confirmed the ability of *Lion* to meet the demanding requirements of precision landing for the Moon application, with a Technology Readiness Level of 3. The *Lion* design and performance is the subject of a PhD thesis [12]. The present paper focuses on a possible step-wise validation approach for AVN systems and its application to *Lion*.

2. LION FUNCTIONAL ARCHITECTURE

We only remind here the *Lion* functional architecture which has been presented in [1] and [4] and which is extensively described in [12]. *Lion* involves two processes : an offline process (fig. 2.1) and an online process (fig. 2.3).

Offline Process

The *offline* process prepares a database of landmarks (also referred to as a "Map") to be used for on-board matching of the extracted features points. This process involves the use of high resolution imagery and DEMs, with associated registration data, obtained from previous orbital missions. This is the case for the Moon (LRO and Kaguya images, LOLA altimeter) and for Mars (MRO, Mars Express and MOLA altimeter), which are the main targets of *Lion* ; for other missions (such as orbiting comets or asteroids), such data is not available a priori, but an initial mapping phase is usually planned for such missions, in which the database could be built (e.g. ROSETTA).

High resolution images of the expected flyby area are selected, as well as the associated DEMs of the surface ; the required resolution of the orbital data depends on the expected on-board camera pixel footprint and therefore will become more stringent as soon as the camera gets closer to the surface.

Typical requirements on required orbital data resolution are summarised in table 2.1. For instance, LRO and MRO missions both provide image with resolutions better than 1m. They assume the orbital data needs to be at least twice as accurate as the descent image to avoid aliasing effects.

Altitude [km]	Descent Camera pixel footprint [m]	Required orbital data resolution [m]
100	119	60
10	12	6
1	1.2	0.6

Tab. 2.1. Typical required Orbital Data resolution for use of Absolute Visual Navigation with a 70-deg field of view camera with 1024x1024 pixels.

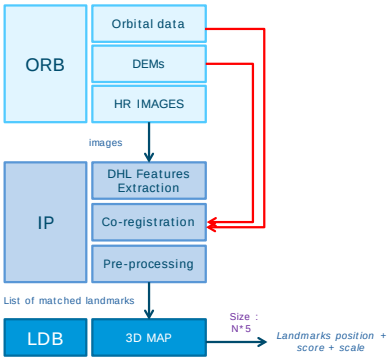

Fig. 2.1. *Lion* absolute visual navigation system functional architecture (offline process).

Harris-Laplace has been selected as feature extractor. The detailed motivation can be found in [1] but can be summarised as : first, there is strong European heritage on the use of Harris-based algorithms, such as the Features Extraction Integrated Circuit implemented on NPAL camera [7] and secondly, the Harris-Laplace provides scale-invariance while allowing to add a parameter to the descriptor associated with each feature : its scale.

One of the main drawback of standard Harris-based features extractors is their sensitivity to the change of altitude between the orbital and the descent images, even under similar illumination. Indeed it is crucial to maximize both the repeatability of the landmarks between orbital and descent images and the spatial distribution of features for good navigation performance. For that purpose, a distributed extraction scale-invariant step has been implemented, which consists in dividing the orbital image in 9 sub-images of equal size, and applying the Harris Laplace extraction on each sub-image. The principle consists in selecting the local Harris-Laplace maxima on each of the sub-image down to a certain score threshold ratio, instead of the absolute maxima at image level.

The number of sub-images has been tuned empirically to 9. This approach brings an increased robustness to the Lion system, in particular to very different illumination conditions as presented in §6.

The implemented features extraction is hereafter referred to as DHL for Distributed Harris Laplace.

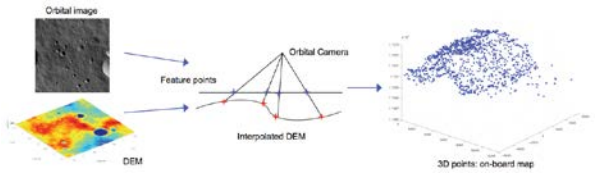

Fig. 2.2 *Lion* landmarks database generation process.

Online Process

The *online* process includes the on-board image processing (IP) and absolute visual navigation (AVN) functions required to estimate the state of the S/C. The details on the actual design can be found in [1].

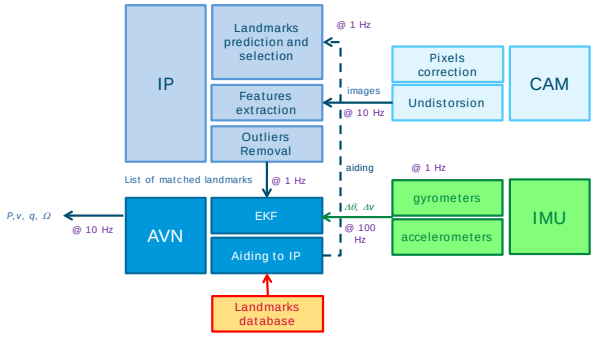

Fig. 2.3. *Lion* absolute visual navigation system functional architecture (online process).

Prior to the image processing itself, some low level corrections need to be performed on the images acquired by the camera, such as pixel correction (not implemented in Lion) and undistorsion of images based on the calibrated intrinsic parameters of the camera.

Image Processing task includes 4 subsequent steps :

(1) *Landmarks prediction.* The prediction step uses the navigation aiding information (the current state covariance matrix and the list of visible landmarks in the FOV) to predict the position, scale and a search area for each of the landmarks in visibility in the current descent images, with no flat-terrain assumption.

(2) *Landmarks selection.* The selection step removes potential landmarks ambiguities (when search areas of 2 landmarks overlap, then only the one with the highest score is selected)

(3) *Features extraction and matching*. The extraction step computes, for each selected landmark, the "cornerness" at the predicted scale over the whole search area in the descent image. The position of the pixel with the highest cornerness value is chosen as a match for the landmark.

(4) *Outliers removal.* A standard RANSAC algorithm is used, which randomly selects sets of 3 match pairs from which a camera model can be computed, counts the number of other matches which agree with that model, and repeats this process a sufficient number of times to ensure with a probability of more than 99% that the model with most inliers is the correct one. Associated inliers form the final set of matches which is fed as a measurement to the navigation filter.

Navigation filter

The Navigation architecture combines an extended Kalman filter and an aiding function. The filter architecture relies on a sliding-window with 1 window, to cope with image processing delay only. Hence the state includes 21 components : 15 components of the state are the current position error in planetary fixed frame, velocity error in planetary fixed frame, and attitude error with respect to planetary fixed frame, accelerometers and gyrometers biases ; the state is augmented with the latest camera pose error estimate to cope with potential delays. This results in a state with 21 components.

Navigation Aiding

Based on the knowledge of the current estimated pose of the camera with respect to the surface, the Navigation filter predicts the landmarks which are visible in the field of view of the camera, as well as their scale in the descent image. This list of pre-selected landmarks, as well as the current state covariance matrix, are provided to the Image Processing as an aiding to the matching process. This a key element in the design as it allows to look only for landmarks in search areas around their expected location and at their expected scale. The heavy task to extract landmarks at each scale in the image is therefore deported towards the offline process, for which processing time is not critical.

3. STEP-WISE VALIDATION APPROACH FOR AVN

Challenges of AVN validation

Challenges of precision landing lie not only in the required navigation accuracy (100 m absolute positioning, only a factor 10 increase with respect to GPS on Earth), but also on its validation in a "representative environment", which is required to raise the Technology Readiness Level (TRL) of such a technology : since AVN techniques rely on the actual terrain visual properties (texture, illumination,

reflectance, radiometry, etc…), which have no Earth analogues (especially for the Moon), how can we consolidate the TRL level to the required level prior to the mission itself ? The answer to this question is not easy, and requires the complementary use of the following data sources:

- Existing imagery data from past orbital missions (provided usually by payload instruments) such as LRO, MRO. The main limitation of such data is the limited coverage at high resolution of the planetary surface, the limited knowledge of the payload characteristics at the origin of the data, and the limited knowledge of the ground truth of the spacecraft when data was acquired.
- Synthetic planetary scene data generated with dedicated rendering tool (PANGU, [13]), allowing to play with illumination conditions, terrains types, textures and error sources. The main limitation of such an approach is that it does not take into account the camera sensor itself (detector response, motion blur, integration time).
- Indoor facility field images of a terrain with high accuracy ground truth (gantry robot and planetary mock-up). Such set-ups allow to address the impact of real camera on the navigation performance, and to consolidate the landing navigation error budget on planetary-analogue surfaces.
- Outdoor facility field images with dedicated UAV. Although it is difficult to find planetary-analogue terrains on Earth, UAV flights allow to play dynamic scenarios with IMU in the loop, which can not be performed in indoor facilities, allowing to test the full visual navigation chain.

Data	**Sensors**	**Terrain type illumination coverage**	**Ground truth**
Past missions imagery	Real CAM Limited knowledge	Real terrain Limited area Artefacts	Limited (for LRO : 60m overall, 10m over the poles)
Virtual images	Ideal CAM	Any coverage, any illumination	Ideal ground truth
Indoor facility images	Flight-like CAM	Planet-analogue terrain Limited coverage	Millimeter accuracy
Outdoor facility images	Flight-like CAM Flight-like IMU	Non-representative terrain and illumination representative dynamics	10 cm typical accuracy (DGPS)

Fig. 3.1. Possible image data sources for AVN validation

Incremental validations strategy for LION

The *Lion* navigation system prototyping has followed a step-wise incremental approach to validate the full navigation chain, including real sensors (IMU, camera), navigation filter and image processing algorithms.

The 4 steps adopted for *Lion* step-wise validation (illustrated in Fig. 3.2) are the following :

1. Point-based simulation
2. Virtual -image generation
3. Indoor Lunar test bench
4. Terrestrial UAV flying test bench

	NAV chain validation	IMU	Camera	NAV	IP
1	NAV	simulated	None	Real	Simulated
2	NAV+IP	simulated	Virtual	Real	Real
3	NAV+IP+ CAM	simulated	Real	Real	Real
4	NAV+IP+ CAM+ IMU	Real	Real	Real	Real

Fig. 3.2. *Lion* step-wise validation approach

Step 1 aims at validating the navigation filter core design. It consists in bypassing the image processing by generating points to emulate the extracted features. IMU data is also simulated.

Step 2 integrates the image processing and the navigation filter. Image processing is based on virtual images of the expected planetary surface generated with PANGU [13], and coherent with the real pose of the camera along a realistic landing trajectory. IMU data is simulated.

Step 3 includes a real camera sensor, representative of space equipment. To face the camera, either an optical simulator or a real terrain are required. A 1024x1024-pixel camera with 70-deg field of view is selected for this purpose. The VisiLab testbench is selected as real terrain (the testbench itself is described §4). However, no flight-representative inertial data can be obtained by fing an IMU to the camera support in Visilab because the signal-to-noise ratio cannot be scaled to a landing mission. Indeed, specific forces and angular rates sensed in the laboratory would be much smaller than in the actual flight while the noise and bias would be of the same order of magnitude. IMU data is simulated.

Step 4 : To validate the full AVN chain, including the real IMU, requires an actual flight on representative dynamics. UAV are promising vectors to embark a vision-based navigation experiment, as it has been

demonstrated with NPAL camera on-board the PLGTF unmanned helicopter [7], although such a validation may suffer from excessive vibrations which need to be taken into account when designing the experiment (and modelled).

Next steps will require HW implementation and real-time prototyping of *Lion* and will be subject of a future activity. The AVN system could then be merged with other Landing GNC building blocks for subsequent maturation of the overall GNC integration readiness level, according to the overall GNC validation strategy described in [5]. The proposed AVN validation approach is summarised in Fig. 3.3.

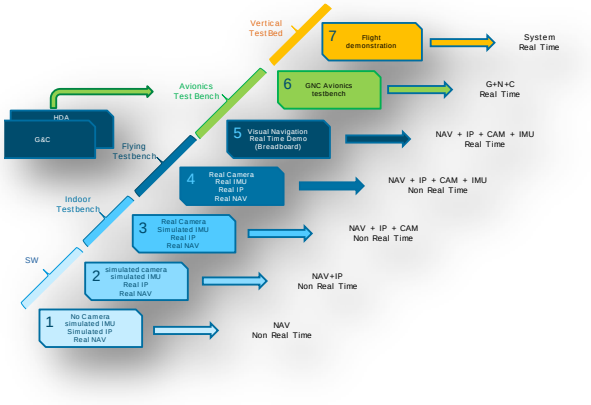

Fig. 3.3. Illustration of step-wise integration approach for a Visual Navigation System. *Lion* has been integrated up to the level 4.

The current validation step, which is the main subject of this paper is the number 3 with the validation on a Lunar-analogue testbench : VisiLab.

4. 'VisiLab' VISION-BASED NAVIGATION TESTBENCH DESIGN

Visilab is a vision-based navigation test bench located at ESA-ESTEC in Noordwijk (The Netherlands). It includes a lunar-analogue planetary mock-up, a camera mounted on a robotic arm, an illumination system and a calibration framework.

Visilab was designed with three main objectives :

- (1) To allow for a comprehensive understanding of end-to-end error contributors to vision-based navigation systems, including offline and online processes, for pinpoint and safe landing applications.
- (2) Hardware-in-the-loop prototyping and testing of vision-based navigation and hazard detection systems, allowing to meet the step 3 of the step-wise approach (Fig. 3.3)
- (3) The characterization of vision-based camera sensors and the impact of different detectors technologies (rolling or global shutter) on image processing performance.

Planetary Mock-up specification

It was chosen to select the Moon as first validation terrain for *Lion*, due to the availability of accurate orbital data from LRO mission [14].

As guideline for the selection of the DEM, it was decided to only use DEMs based on real data, with no or little need for post-processing so as to obtain a terrain model as representative of the true Moon as possible ; it was also decided not to rely on any planetary scene generator (such as PANGU or equivalent) to build or process the DEM, and this to completely decouple the step 3 of validation from the step 2 (relying on PANGU-generated images). A zone around the South Pole was selected for its interesting topography (craters, mountains) and its scientific interest for future Lunar missions.

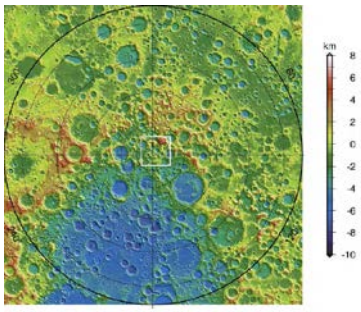

Fig. 4.1. LRO DEM of the Lunar South Pole. In the white rectangle : the extracted DEM for VisiLab.

LRO, which has been orbiting the Moon since 2009, has provided various DEM of the South Pole with excellent resolutions from 5 to 400m. Unfortunately the best resolution also corresponds to the presence of artefacts in the digital elevation model such as trenches, peaks and holes, due to Laser false measurements. The non-visibility of the artefacts in the DEM thus became the sizing driver for the DEM resolution.

A 400-m resolution DEM was therefore selected from altimetry data of the NASA Lunar Reconnaissance Orbiter mission (LRO), representing a surface of 960x1920 km on the Moon around the South Pole. The test bench needed to fit in a reduced available

space of 2x1 m within ESTEC's Control Hardware Laboratory, driving the mock-up specification, in particular in terms of resolution. The DEM has therefore been scaled to the physical dimensions of the mock-up as illustrated in Fig. 4.2.

Exact mock-up dimensions	980*1960 mm
Milling line step	0.5 mm
Maximum height range	50 mm
DEM resolution	1960*3920
DEM resolution depth	16 bits
Equivalent Lunar dimensions	960*1920 km
DEM Lunar Pixel Footpring	490 m

Fig. 4.2. Lunar-analogue mock-up specification

Planetary Mock-up realization

The DEM data specified by ESA was processed by DLR to agree with the manufacturer's requirements and supported with accompanying data such as material choice, milling track distance, milling direction and milling head size. Furthermore several grooves at the back side and in the side planes have been defined for supporting the later assembly. The milling was done in three steps, beginning with two coarse milling steps. Fig 4.3 shows the application of the last fine milling step. The manufacturing process is the one put in place for the TRON facility [17].

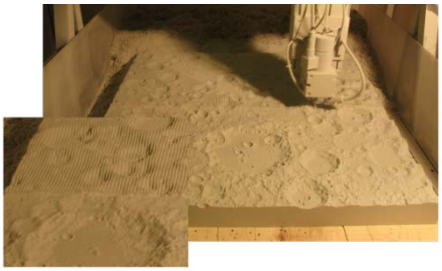

Figure 4.3: VisiLab planetary mock-up tile at fine milling stage

Camera support design

The camera support requires at least 4 degrees of freedom: 3 translations, and 1 rotation about the pitch axis to simulate a realistic Lunar trajectory although not fully representative. A camera support had to be designed to provide this motion capability. The design relies on the initial equipment available in the laboratory and shown in Fig 4.7: a motorized translation table with a 92-cm course. The translation table was designed within ESA for previous projects and can be controlled to a 0.1-mm position accuracy along the axis. The other non-motorized translation axes were added, allowing to adjust the position at sub-millimetric level thanks to dedicated micro-metric screw. Although fully motorized 6-dof capability would be desirable for mimicking a Lunar trajectory, this capability was not available in the laboratory in the frame of the project. However, since the purpose of this validation campaign was not to demonstrate in real time the *Lion* performance, but to acquire images all along the expected trajectory, representative of a 1 Hz image frame rate acquisition, it was acceptable to perform image acquisitions at pre-defined positions on VisiLab, coherent with a 1 Hz image acquisition rate at scale on the selected descent trajectories.

The camera support and the mock-up are both mounted on a highly stable optical table which is about 2.5 m long and 1.2 m wide .

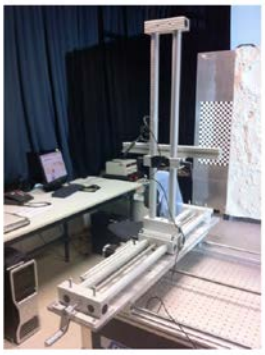

Fig. 4.4 VisiLab camera support structure.

Planetary mock-up support design

A highly stable supporting structure for the planetary mock-up has been designed and assembled at ESA, allowing to rigidly attach the mock-up and the camera on a ultra-stable optical table. The main architecture choice was to mount the mock-up vertically, to allow for the use of the horizontal translation table for accurate positioning. The mock-up supporting structure is shown in Fig. 4.5.

Figure 4.5: VisiLab supporting structure for the Planetary Mock-up

Illumination system

Accurate modelling of Lunar-like illumination conditions require :

- (1) White light (Sun-like)
- (2) Parallel light rays (Sun is at infinity)
- (3) Uniform surface flux

Although the first 2 requirements can be met thanks to the use of a collimated light beam (for example : halogen lamp placed behind a Fresnel lens), the 3rd one is not easy to meet in a small laboratory, especially the uniformity of the flux.

A simple retro-projector with a 500-W lamp was available in the premises at ESTEC, which relies on the same optical scheme as a Fresnel lens, and was used as the illumination system for Visilab as it renders realistic images, with a known limitation due to finite distance of operation. The impact of this physical limitation is addressed in the Experiment Results chapter.

5. 'VisiLab' calibration and scalability analysis

Scalability Analysis

The key driver for scaling a planetary landing scenario to a laboratory environment is the ground truth knowledge, which can be defined as the absolute knowledge of the real camera pose at the time when each image is acquired. If the knowledge of the ground truth is poorer than the navigation performance (at scale) we want to observe, then the test bench is useless. Hence, a significant effort has been devoted to the characterisation and refinement of the ground truth, as described below. This involves 2 aspects : the accurate calibration of the planetary mock-up itself (DEM accuracy) and the calibration of the test set-up itself.

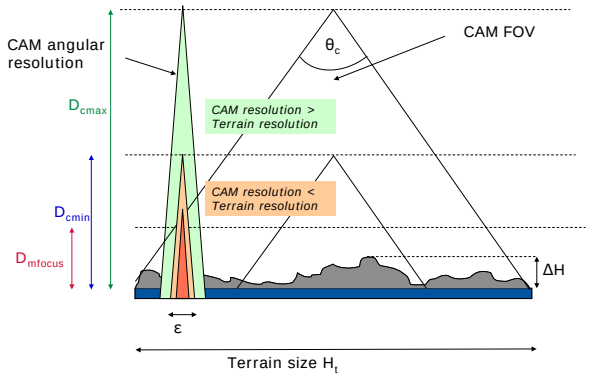

Fig. 5.1. Illustration of key distances in VisiLab for scalability analysis.

To perform a proper scaling, the limitations of the testbench need to be taken into account (Fig. 5.2), and the following elements have been considered :

- The maximal distance from mock-up to the camera is ~1 m (width of the optical table)
- The minimal distance from mock-up to the camera is ~6 cm (minimal focused distance)
- The targeted navigation performance on a Lunar landing scenario is better than 100m
- The targeted domain of use of AVN technique is typically betwee 1 and 100 km of altitude

The trade-off on the scale factor selection is illustrated in Fig. 5.2 below : it has to be between 1e-5 and 1e-4 typically to cover the expected range of use while requiring a ground truth knowledge of a minimum of 1 mm, compatible with VisiLab ground truth measurement needs. With this scale factor also, the manufacturing resolution of the mock-up itself is one order of magnitude better than the specified DEM resolution at scale, which ensures the observed scene remains representative of a real Lunar scenario, from terrain resolution perspective.

	SCALE FACTOR				
	1.00E-07	1.00E-06	1.00E-05	1.00E-04	1.00E-03
Initial DEM resolution [m]	4.00E+02				
NAV performance [m]	1.00E+02				
Requirement on ground truth accuracy [m]	1.00E-05	1.00E-05	1.00E-03	1.00E-02	1.00E-01
DEM manufacturing precision at scale [m]	5.00E+03	5.00E+02	5.00E+01	5.00E+00	5.00E-01
MAX range [km]	1.00E+04	1.00E+03	1.00E+02	1.00E+01	1.00E+00
MIN range [km]	6.00E+02	6.00E+01	6.00E+00	6.00E-01	6.00E-02

Fig. 5.2. Trade-off on scale factor for a Lunar Landing scenario.

Planetary mock-up calibration

After delivery to DLR Bremen the two tiles have been assembled and the result has been laser scanned for calibration. This calibration is required to describe the actual geometry of the terrain model with respect to a reference system which must be determinable in VisiLab with a high repeatability.

Therefore a physical reference system was defined so that its origin rests at one lower corner of the terrain model. The Z direction is defined to be perpendicular to the back plane of the model, X and Y directions pointing along the mock-up edges.

The scanning took place on a massive stone table which possesses a micrometer precise flatness, thus providing an ideal ground for resting the assembled terrain model. For scanning the Laser Tracker system AT901-MR in combination with the T-Scan tool was used (seeFig. 4.4). Both tools belong to the toolchain of the Testbed for Robotic Optical Navigation (TRON)

which is located in DLR Bremen. After processing of the scan data the DEM of the actual terrain model was determined and stored as TIFF file with a resolution of 3920 x 1960 pixels, thus providing a physical resolution of 0.5 mm per pixel. Also the transformation from the DEM to the physical reference system could be determined. The surface scan precision is 0.2 mm MPE.

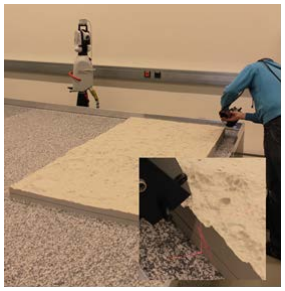

Figure 5.3: Scanning of terrain model, laser tracker in background. close-up shows scanner and red laser pattern

End-to-end mock-up realization error

The scanning data allowed an analysis of the end-to-end accuracy of the complete process chain starting at the ESTEC's theoretically derived DEM, going further to manufacturing, delivery, assembly, laser scanning and scan data processing. For determining the accuracy the scanned DEM was substracted from the specified reference DEM pixel by pixel. The result is shown in Fig 4.5.

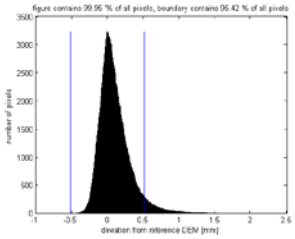

Fig 5.4: End-to-End accuracy analysis for the process from reference to ground truth DEM. 95.4 % of all scan points are with 0.5 mm accuracy.

It can be seen that the manufactured model tends to be higher than defined by the reference model. The reason for this behavior is a physical limitation due to the spherical geometry of the milling head. Therefore features such as very steep terrain or very small, deep craters could not be manufactured. Even with this limitation 95% of all pixels have a realization error much smaller than 0.5 mm with respect to the specified DEM.

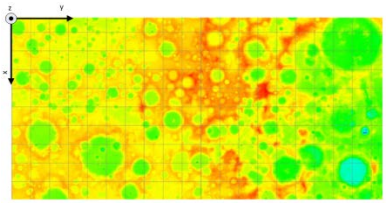

Fig. 5.5 VISILAB calibrated DEM of the planetary mock-up.

Ground Truth knowledge

As stated above, a driver for the test-bench usefulness is the ability to calibrate the actual pose of the camera very accurately, at mm level with the expected scale factors. The ground truth error is the combination of all errors contributing to the frame transformation from mock-up fixed frame to camera-fixed frame. A 2-step calibration of the camera pose has been implemented to meet the 1-mm ground truth accuracy requirement.

First calibration step.

The first step consists in using a calibration grid pattern to evaluate intrinsic camera parameters, and a partial estimate of its extrinsic parameters, providing a pose estimation of the camera in calibration configuration. The Bouguet method [9] has been used for this purpose. The calibration error as observed in VisiLab is estimated to be 0.7mm per axis (3 sigma) and 0.1° per axis (3 sigma).

This error needs to be propagated to the camera acquisition position based on support structure repeatability error.

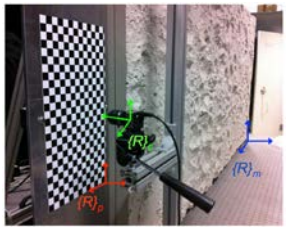

Fig. 5.6 Camera in calibration position

The intrinsic repeatability of the camera support has been evaluated by specific tests (consisting in moving back and forward the support and performing a visual calibration at each iteration) and evaluated to 0.2 mm (3 sigma) per axis and 0.17° (3 sigma) per axis.

Combined with the misalignment of the camera support with respect to the mock-up, and the calibration-pose error, this leads to a total pose estimation error at image acquisition (worst case) of typically 4.5 mm and 0.5° per (3-RMS). With the scale factors selected, this accuracy is not sufficient and a refinement step is required.

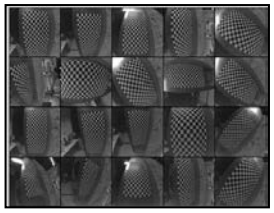

Fig. 5.7. Camera calibration pictures based on [9]

Second calibration step

Since the DEM of the planetary mock-up is known one order of magnitude better than the required ground truth accuracy, the idea is to exploit the DEM to refine the visual calibration of the first step, by calibrating directly the camera with respect to the DEM, hence getting rid of all the errors contributors linked to the support structure, which were driving the 1st step calibration error. Scene rendering tools, such as PANGU [13], developed by University of Dundee under ESA contract, allow to generate 2D views of a given 3D terrain for any camera pose.

The implemented approach consists in generating a virtual image of the scene with Pangu, based on the pose estimation obtained at first step. This image is then matched with the real image taken, and the geometrical transformation from virtual to real image provides a refinement of the pose.

To avoid any functional link with the AVN technique to be validated, different features extraction and matching technique have been used, based on SIFT features [15], with an outlier removal based on the EPnP algorithm using 6 points randomly selected among 1000 matches [12].

The second step allows to improve drastically the ground truth in camera acquisition position, to a level acceptable. The final error is 0.65 mm and 0.05° (including mock-up DEM accuracy).

	Position [mm] (3-RMS)	Attitude [°] (3-RMS)
Step 1	4.5	0.5
Step 2	0.65	0.05

Fig. 5.8.Ground truth accuracy

At the end of this calibration effort, the estimated accuracy is :

- 0.2 mm for the knowledge of the terrain (per axis, considered 3 –RMS)
- 0.65 mm and 0.05° for the knowledge of the real camera pose

6. EXPERIMENTAL RESULTS

Scenarios definition

A standard lunar descent scenario starts from parking orbit at 100 km of altitude. The whole trajectory can be considered to be in the orbital plane. After performing system checks, the lander commits to a ballistic descent around half of the lunar circumference down to a 10-km altitude when the main engines are started. From there the so-called braking phase begins. It aims at canceling the orbital velocity in a fuel-optimal way before analysing the landing site surroundings and avoid hazards during the approach phase. AVN can be used during the whole phase, from coasting phase down to few km altitude. This typical trajectory has been selected to validate the *Lion* algorithm and implemented in VisiLab. Based on the Scalability analysis, 5 scenarios have been defined and run on VisiLab for the assessment of *Lion* performance, each one corresponding to ~30s of flight at key points of a Lunar landing trajectory. Complete test campaign details and result analysis can be found in [12]

The landmark database has been generated based on the following VisiLab data :

- For scenarios 1.1 and 1.2 : a low resolution image has been acquired, with a resolution (100m/pixel at scale) comparable with available LRO data at low latitudes.
- For scenarios 2.1 and 2.2 : a high resolution images has been generated, with a resolution of 25m/pixel (a bit worse than available LRO NAC imagery at high latitudes)
- For scenario 3 : a high resolution image has been generated, with a resolution of 6.25 m/pixel

The 3 orbital images have been generated with the same camera as the “descent” images, but with different lenses.

PARAMETER	**SCENARIOS 1.1 AND 1.2**	**SCENARIOS 2.1 AND 2.2**	**SCENARIO 3**
Altitude [km]	100 and 50	15 and 10	From 5 to 3
Scale factor VisiLAB/Real	8.5e-6	4.1e-5	1.2e-4
Coverage	Global	Global-Pole	Pole
Terrain Resolution [m]	59	12.1	4.2
Ground Truth Knowledge (3σ) [m]	76.7	15.7	5.5
Low Resolution Orbital Image [m]	100	100	100
High-Resolution Orbital Image	N/A	25	6.25

Fig. 6.1. Scenarios definition and contribution of testbench intrinsic resolution (0.5 mm) and ground truth knowledge (0.6 mm), scaled to each scenario

Navigation Performance

On each of the 5 sequences of images acquired on VisiLab, the *Lion* algorithm is tested statistically by dispersing the initial position, velocity and attitude estimation errors, assuming a Gaussian dispersion. The 3sigma dispersions considered at initialization are voluntarily conservative for a Lunar scenario:

- 0.5 m/s in velocity estimation per axis
- 5% of initial altitude on the position estimation per axis.
- 0.5° in attitude per axis

Note that these initial estimation errors can easily be provided by Ground-based orbit determination and the on-board Star Tracker.

The performances obtained for each sequence are summarised in Fig. 6.3.

The results obtained with real images and with a limited ground truth knowledge confirm the very good performance of the *Lion* system, fully in line with precision landing requirement of 100m.

These experimental results can be correlated to the resolution of the available orbital data and to the ground truth. The mean error is clearly dominated by the ground truth error at low altitudes, while at higher altitudes the descent image resolution becomes the driving contributor. The navigation standard deviation increases non linearly with the descent image resolution.

Since in the best case 6.25m orbital resolution has been used in VisiLab whereas real orbital images may reach 0.5 m resolution (at least for the Moon and for Mars) above landing sites of interest, an improvement of this performance can be reasonably assumed for future landing missions.

	100 KM	50 KM	15 KM	10 KM	3 KM
Mean position error [m]	139	80	75	18	4
3-RMS dispersion [m]	980	350	176	130	47
Descent Image Resolution [m]	119	60	18	12	3.6
Orbital Image resolution [m]	100	100	100	25	6.2
VisiLab Ground truth knowledge at Scale [m]	77	77	77	16	5.5

Fig. 6.2 Statistical distribution of navigation performance at the end of each 30s sequence, obtained with a random normal distribution of initial position, velocity and attitude (respectively 5% of the altitude, 0.5 m/s and 0.5° per axis).

Note that in the 100 km case, the convergence has not been fully reached at the end of the 30s sequence, such that the performance indicated for that case is not fully representative of the converged performance.

Robustness cases

Influence of orbital data image sensor knowledge.

The quality of orbital data is important for the performance of an AVN system like *Lion*. This is especially important for the orbital image which is used to extract the landmarks to build the reference map. To simulate an ideal orbital image, PANGU has been used to generate an ideal orbital image (low resolution case) from which the database is generated ; the online navigation performance is then compared with the above scenarios based on the baseline landmark database. Both images have been co-aligned with an overall accuracy of 0.65mm and 0.05° (following the same method as in §5).

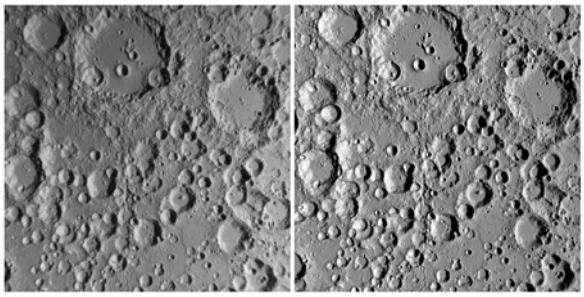

Fig. 6.3 The 2 orbital images used for robustness assessment. Left : VisiLab image. Right : PANGU image.

The results show a typical 50% degradation of the overall navigation error dispersion at all altitudes due to the use of the real orbital imagery

	TOTAL ERROR 3-RMS [M]
Ideal Orbital Image	97
Real Orbital Image	155

Fig. 6.4 Robustness to orbital camera sensor. Navigation performances are compared here at an altitude of 20 km obtained with the HR image.

These errors can not be fully explained by the known misalignment between images (0.65mm and 0.05° represent a total pose uncertainty of the orbital image of 33m at scale and at 20 km altitude). An additional error is linked to the camera properties itself. In

particular, the distortion of the images needs to be corrected thanks to the calibration method described §5, which is of course not perfect in itself, and introduces a blurring of the corrected images close to the border.

To assess the impact of inaccurate camera calibration, a sensitivity test has been performed by voluntarily degrading the calibrated intrinsic parameters by 5% and comparing the location of Harris feature points in the obtained images, after rectification. Results are illustrated in fig 6.5.

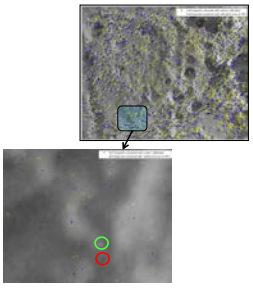

	calibration
Image Size, [nx ny]	[1024 1280]
Focal Length, fc [pix_x pix_y]	[694.37 694.45]
Principal point, cc [pix_x pix_y]	[637.99 535.03]
Skew coefficient, alpha_c	[-0.00016]
Distortion coefficients, (kc)	[-0.372 0.206 -0.0003 -0.0003 -0.071]

Fig. 6.5 Assessment of the impact of 5% calibration errors on feature points location.

The impact of calibration errors on feature points location has been estimated by visual inspection on a typical VisiLab image, with 2 types of features extractors : SURF and HARRIS, leading to locally significant excursions of features points, although if globally the biggest displacements are observed close to the edges, where the residual distortion is maximal.

ERROR	HARRIS	SURF
< 1 pixel	6%	7%
Between 1 and 3 pixels	15%	18%
> 3 pixels	79%	75%

Fig. 6 .6 Impact of 5% calibration error on features location. A +5% error has been added on all calibrated intrinsic parameters.

Although 5% dispersion on all calibration parameters might be way too conservative, this sensitivity test shows the impact of camera calibration on features position in the image. This might be critical for the orbital image which is used to generate the landmarks database, and might explain the differences

Impact of finite distance illumination source

The main limitation of VisiLab testbench, like any finite-size ground testbench, is the representativity of the illumination system. Indeed, unlike the Sun, the illumination system of VisiLab is at a finite distance from the planetary mock-up ; since the received intensity decreases quadratically with the distance to the light source, this will generate a gradient in light intensity flux on the mock-up. This might be problematic for the tested navigation system since in particular Harris features are sensitive to these gradients. The flux at a distance r of a light source is given by :

$$\Phi(r) = \frac{K}{4\pi r^2} \qquad (1)$$

Where : K is the light-source power and r the distance to the source. The flux variation over the full mock-up width δr is can therefore be approximated by :

$$\frac{\Delta\Phi(r)}{\Phi(r)} = \frac{-2\delta r}{r} \quad (1)$$

On a real Moon Landing scenario, this flux variation over a similar terrain would be typically 1 ppm (worst case). In a 1m size mock-up with a light source located at a maximum of 5m, the flux variation is bigger than 50% : this is an intrinsic limitation of a ground facility for the validation of vision-based system. To assess its impact on the *Lion* assessment, the following test has been performed :

- (1) An image of the planetary mock-up has been acquired with the VisiLab camera.
- (2) Based on the DEM of the planetary mock-up, the expected image of the same scene has been rendered based on the PANGU scene generator, assuming a Lunar-like lightning environment.
- (3) Both images have been compared in terms of radiometry and intensity.
- (4) The *Lion* image processing algorithms have been compared on both images in terms of number of matches and their distribution.

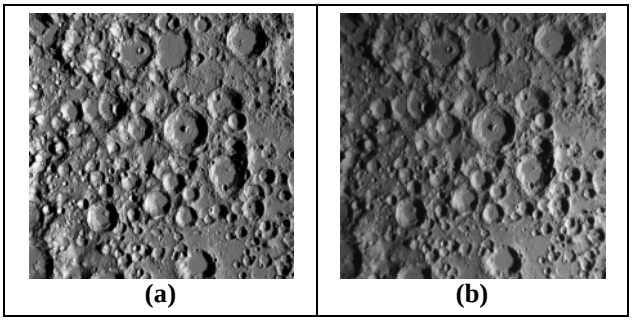

Fig. 6.7. Raw images of the VisiLab testbench. (a) rendered with PANGU based on calibrated DEM. (b) real rectified image.

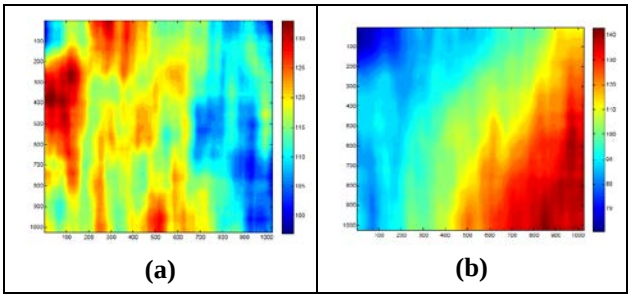

Fig. 6.8. Intensity of the image expressed in grey levels. (a) virtual image rendered with PANGU. (b) real image.

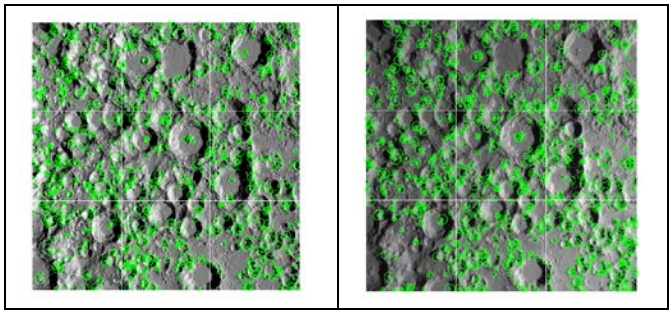

Fig. 6.9. Distributed Harris-Laplace features. (a) virtual image rendered with PANGU. (b) real image.

Despite significant differences in terms of flux variations, the repeatability figures between the PANGU ideal image and the real image for the distributed Harris-Laplace features is close to 80% which, from an Image Processing point of view, is deemed very good. This is because the Harris-Laplce extraction is only concerned with local image gradients at the feature scale, over which the global flux variation due to the finite-size illumination has negligible impact.

As a consequence, the intrinsic limitation of the testbench due to the finite distance of the light source has no noticeable impact on the *Lion* image processing and navigation performance.

7. FUTURE WORK

UAV flight test

The use of Harris-Laplace features in *Lion* is motivated by the fact that they are generic enough to be detected on any type of textured terrains, whatever the celestial body explored. Since *Lion* was only tested in lunar conditions so far, it would be interesting to get test results representative of another environment. In addition, testing on real flight data would allow to test the robustness of the image processing to vibrations and validate the inertial propagation model since a real IMU could not be used at scale in VisiLab, thus validation step 4 in Figure 3.3. All these aspects could be tested through an helicopter UAV terrestrial flight experiment which was run in February, 2013 on the Caylus site near Toulouse by the ONERA UAV flight team. The orthoimage and the DEM are at a 20-cm resolution [16]. The trajectory shown in Fig. 7.1 involved several horizontal passes at different altitudes to test robustness to scale changes, another low altitude manual flight over houses was done to test robustness to 3D terrains. Testing *Lion* on these data is planned as a follow-on work at ESA-ESTEC. It can be related to previous absolute visual navigation UAV flight experiments by Trawny et al. [11].

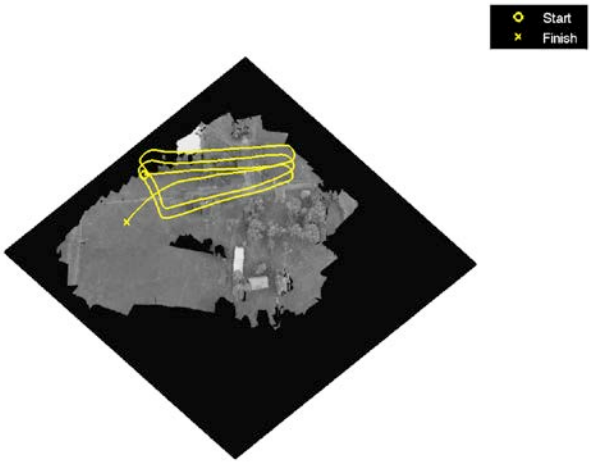

Fig. 7.1. Helicopter UAV test flight trajectory sample over the Caylus site near Toulouse, France.

Conclusion

Overall, the step-wise validation approach which has been applied on Lion has allowed the prototyping and successful validation of the Lion navigation system, demonstrating in particular that its performance was perfectly in line with the precision landing requirement of 100m at touch-down, confirming the previously established results obtained by simulation with virtual images [1]. The detailed design and performance report of Lion can be found in [12].

Compared to purely SW tests, VisiLab has shown its usefulness by putting in evidence the impact of the sensors used to acquire both orbital and descent images on the final navigation performance. A sub-millimetric ground truth accuracy of the VisiLab testbench was key in achieving this.

The approach has also demonstrated the strong interest of a small-size and high accuracy vision test bench for validating and early prototyping of vision based navigation algorithms.

Next validation steps will include the validation of Relative Visual Navigation techniques in complement of *Lion* to perform an end-to-end characterization of a Visual Navigation System from orbit down to Landing on the VisiLab testbench. This will include the real time prototyping of the algorithms and their implementation on a real time avionics testbench, to assess the compatibility of Lion with landing mission needs, not only from navigation performance standpoint, but from real time implementation.

8. ACKNOWLEDGEMENTS

The authors would like to thank Bolko Maass from DLR ; Phil Airey and Daniele Baker Wilson from ESA for their contribution in the design and use of the VisiLab testbench, Martial Sanfourche from ONERA for his contribution to selecting the VisiLab camera, and finally Paul Chavent from ONERA too for helping design and running the UAV flight experiment.

9. REFERENCES

1. Delaune J., et al., Optical Terrain navigation for pinpoint landing : image scale and position-guided landmark matching" (AAS 12-087), American Astronautical Society Guidance and Control Conference, Breckenridge, USA, 2012.

2. Simard Bilodeau S., et al., Pinpoint Lunar Landing using crater detection and matching : design and laboratory validation, *AIAA Guidance, Navigation and Control Conference*, Minneapolis, USA, 2012.

3. Van Pham B., et al., Fusion of visual odometry and landmark constellation matching for spacecraft absolute navigation : analysis and experiments, *11th Symposium on Advanced Space Technologies in Robotics and Automation*, Noordwijk, the Netherlands, 2011.

4. Delaune J., et al., "Camera-aided inertial navigation for pinpoint planetary landing on rugged terrains", *International Planetary Probe Workshop*, Portsmouth, VA, USA, 2011.

5. Philippe C., et al., Validation & Verification Approach for European Safe Precision Landing GNC technologies, *6th International Planetary Probe Workshop*, Atlanta, USA, 2008.

6. Delaunoy A., et al., Multi-view 3D reconstruction of Asteroids, *5th International Conference on Astrodynamics Tools and Techniques 2012*. HAL-00746667.

7. Fischer D., et al., "NPAL evolutions applied to ESA's Lunar Lander mission" (AAS 12-076), *American Astronautical Society Guidance and Control Conference*, Breckenridge, USA, 2012..

8. LRO LOLA archives.
http://imbrium.mit.edu/LOLA.html

9. Bouguet Calibration toolbox
http://www.vision.caltech.edu/bouguetj/calib doc/

10. Sanfourche M., et al., "Perception for UAV: Vision-Based Navigation and Environment Modeling", *Aerospace Lab*, 4, 2012.

11. Trawny N., et al., "Vision-Aided Inertial Navigation for Pinpoint Landing using Observations of Mapped Landmarks". *Journal of Field Robotics*, 24, 2007.

12. Delaune J., "Vision-based navigation for pinpoint planetary landing on any relief", PhD thesis, to be defended in July, 2013.

13. Parkes S., et al.,. Planet Surface Simulation with PANGU. *Eighth International Conference on Space Operations*, Montreal, Canada, 2004.

14. Chin, G., et al., Lunar Reconnaissance Orbiter Overview : The Instrument Suite and Mission. *Space Science Reviews*, 129(4) :391–419, 2007.

15. Lowe, D. G. (2004). Distinctive Image Features from Scale-Invariant Keypoints. *International Journal of Computer Vision*, 60(2) :91–110.

16. Sanfourche, M., et. Al, Perception for UAV : Vision-Based Navigation and Environment Modeling. *Aerospace Lab*, 2012.

17. Krueger, H., et. Al, TRON – Hardware-in-the-loop test facility for Lunar Descent and Landing Optical Navigation. *IFAC*, 2010.